Crystallographic, Theoretical, and Spectroscopic Studies of the Luminescent $d^{10}-d^{10}$ Binuclear Copper Acetate Complex $Cu_2(dppm)_2(O_2CCH_3)^+$

Pierre D. Harvey,* Marc Drouin,† and Tianle Zhang

Département de chimie, Université de Sherbrooke, Sherbrooke, Québec J1K 2R1, Canada

Received November 8, 1996[⊗]

The new $d^{10}-d^{10}$ dimer $Cu_2(dppm)_2(O_2CCH_3)^+$ (as a BF_4^- salt) has been prepared and characterized by X-ray crystallography and by ^1H and ^{31}P NMR, vibrational, and electronic spectroscopy. The compound is luminescent at 77 K but not at room temperature. MO calculations and geometry optimizations have been performed using the EHMO and DFT models, respectively. In the solid state the Cu_2 separation is 2.788(1) Å where $\nu(Cu_2) = 87.7\ cm^{-1}$, indicating the presence of weak Cu···Cu interactions. The MO calculations predict that the lowest energy excited states are MLCT from Cu to phenylphosphine/acetate. These predictions have been confirmed by electronic spectroscopy via a comparison between $Cu_2(dppm)_2(O_2CCH_3)^+$ and $Cu_2(dppm)_2(O_2CC_6H_5)^+$. In solutions, both NMR (^1H and ^{31}P) and luminescence spectroscopies (time-resolved spectra and τ_e analysis) demonstrate the presence of two metal species in solutions: $Cu_2(dppm)_2(O_2CCH_3)^+$ and $Cu_2(dppm)(O_2CCH_3)^+$. The dimer crystallizes in the triclinic space group $P\bar{1}$ with $a = 11.572(2)$ Å, $b = 12.552(2)$ Å, $c = 19.543(3)$ Å, $\alpha = 85.274(12)°$, $\beta = 82.108(11)°$, $\gamma = 68.950(12)°$, and $Z = 2$.

Introduction

d^{10} polynuclear copper complexes generally exhibit rich photophysical properties and recently have attracted some attention on both a theoretical and a spectroscopic level.[1,2] Numerous mononuclear Cu(I) phosphine complexes have also been investigated in the literature for their luminescent properties and their photosensitizing functions such as the conversion of norbornadiene into quadricyclane[3] and the isomerization of *cis*- and *trans*-piperylene.[4] Recently our group[2a] and others[5] have investigated the efficient luminescent excited state quenching of Cu(I) species at room temperature using carboxylate derivatives. McMillin et al.[5] have proposed an exciplex formation in order to explain the emission quenching by these substrates. The proposed structure of this exciplex is a pentacoordinated Cu(I) compound.[5] During the course of our investigations, we prepared and characterized the new dimeric complex $Cu_2(dppm)_2(O_2CCH_3)^+$ (dppm = $((C_6H_5)_2P)_2CH_2$). The fact that this Cu complex is polynuclear and is not luminescent in solution at room temperature but is so at 77 K prompted us to investigate its properties and electronic and molecular structures.

Experimental Section

Materials. The solvents ethanol (Fisher) and 2-methyltetrahydrofuran (2-MeTHF) were purified by standard procedures.[7]

$[Cu_2(dppm)_2(O_2CCH_3)]BF_4$. To a 5 mL methanolic solution of CH_3CO_2Na (0.0292 g, 0.356 mmol, i.e. large excess) was added a 20 mL methanolic suspension of $[Cu_3(dppm)_3(OH)](BF_4)_2$[8] (0.108 g, 0.00704 mmol) under N_2(g) atmosphere. The suspension dissolved, and the colorless solution was allowed to stir for 0.5 h. The solution was then evaporated to dryness. The beige filtrate was redissolved in 3 mL of acetone, and the resulting solution was filtered. The filtrate was then evaporated to dryness. The off-white solid was collected and washed with diethyl ether before drying in vacuo. Chemical yield: 92%. ^1H NMR [$(CD_3)_2CO$]: δ 3.47 (br, CH_2P_2), 2.83 ($CH_3CO_2^-$). IR: ν(CO) 1582 (ν_{as}), 1434 cm^{-1} (ν_s). Crystals suitable for X-ray crystallography were obtained from slow diffusion of pentane through an acetone solution. The compound crystallizes with an acetone solvate molecule.

$[Cu_2(dppm)_2(O_2CC_6H_5)]BF_4$ was prepared as stated above except that $C_6H_5CO_2Na$ was used instead of CH_3CO_2Na. The off-white solid was washed three times with diethyl ether and dried in vacuo. Chemical yield: 90%. ^1H NMR [$(CD_3)_2CO$]: δ 3.61 (br, CH_2P_2), 6.7−7.5 (C_6H_5, complex, phenylphosphine), 7.5−8.4 (C_6H_5, complex, benzoate). IR: ν(CO) 1543 (ν_{as}), 1435 cm^{-1} (ν_s).

Spectroscopic Measurements. Absorption spectra were measured on a Hewlett Packard 8452A diode array spectrometer. The emission and excitation spectra were obtained using a Spex Fluorolog II spectrometer or a PTI LS 100 spectrometer. Part of the emission lifetime measurements were also performed on the PTI LS 100 instrument. The second part of the measurements were performed on the Spex Fluorolog II spectrometer equipped with a Spex 1934 D phosphorimeter setup (for time-resolved spectroscopic measurements). The FT-Raman spectra were measured on a Bruker IFS 66/CS FT-IR spectrometer coupled with an FRA 106 FT-Raman module using a Nd:

* To whom correspondence should be addressed. Tel: (819) 821-7092. Fax: (819) 821-8017. E-mail: pharvey@structure.chimie.usherb.ca.

† Laboratoire de chimie structurale, Université de Sherbrooke.

⊗ Abstract published in *Advance ACS Abstracts,* September 15, 1997.

(1) (a) Li, D.; Che, C.-M.; Wong, W.-T.; Shieh, S.-J.; Peng, S.-M. *J. Chem. Soc., Dalton Trans.* **1993**, 653. (b) Lai, D. C.; Zink, J. I. *Inorg. Chem.* **1993**, *32*, 2594. (c) Ryu, C. K.; Vitale, M.; Ford, P. C. *Inorg. Chem.* **1993**, *32*, 869. (d) Ryu, C. K.; Kyle, K. R.; Ford, P. C. *Inorg. Chem.* **1991**, *30*, 3982. (e) Kyle, K. R.; Ryu, C. K.; Ford, P. C. *J. Am. Chem. Soc.* **1991**, *113*, 2954. (f) Kyle, K. R.; Palke, W. E.; Ford, P. C. *Coord. Chem. Rev.* **1990**, *95*, 35. (g) Henary, M.; Zink, J. I. *J. Am. Chem. Soc.* **1989**, *111*, 7404.

(2) (a) Provencher, R.; Harvey, P. D. *Inorg. Chem.* **1996**, *35*, 2235. (b) Harvey, P. D. *Inorg. Chem.* **1995**, *34*, 2019.

(3) (a) Fife, D. J.; Moore, W. M.; Morse, K. W. *J. Am. Chem. Soc.* **1985**, *107*, 7077. (b) Orchard, S. W.; Kutal, C. *Inorg. Chim. Acta* **1982**, *64*, L95.

(4) Liaw, B.; Orchard, S. W.; Kutal, C. *Inorg. Chem.* **1988**, *27*, 1311.

(5) (a) Palmer, C. E.; McMillin, D. R.; Kirmaier, C.; Holten, D. *Inorg. Chem.* **1987**, *26*, 3167. (b) Stacey, E. M.; McMillin, D. R. *Inorg. Chem.* **1990**, *29*, 393.

(6) See, for example: (a) Zelent, B.; Harvey, P. D.; Durocher, G. *Can. J. Spectrosc.* **1984**, *29*, 23. (b) *Can. J. Spectrosc.* **1983**, *28*, 188. (c) Harvey, P. D.; Zelent, B.; Durocher, G. *Spectrosc. Int. J.* **1983**, *2*, 128 and references therein. (d) Brummer, J. G.; Crosby, G. A. *Chem. Phys. Lett.* **1984**, *112*, 15.

(7) (a) Solvent purification: Gordon, A. J.; Ford, R. A. *The chemist's companion, a handbook of practical data, techniques, and references*; Wiley: New York, 1972; p 436. (b) Perrin, D. D.; Armarego, W. L. F.; Perrin, D. R. *Purifications of Laboratory Chemicals*; Pergamon: Oxford, U.K., 1966.

(8) Ho, D. M.; Bau, R. *Inorg. Chem.* **1983**, *22*, 4079.

S0020-1669(96)01353-5 CCC: $14.00

YAG laser (1064-nm excitation) and a Notch filter (cutoff ~60 cm^{-1}). The spectra were acquired using 200−300 scans and a 4 cm^{-1} resolution.

Computational Details. The molecular orbital calculations were performed using the extended Hückel molecular orbital theory (EHMO).[9,10] These calculations were performed using a modified version of the Wolfsberg−Helmholz formula.[10b] The atomic parameters used for Cu, P, H, and O were taken from the literature.[9,10] The interatomic distances were the average values taken from this work's X-ray results (r(CH), r(CO), r(CC), r(CuO), and r(CuP) = 1.05, 1.25, 1.52, 2.01, and 2.25 Å, respectively), unless stated otherwise. The valence bond angles were taken as ideal for a planar trigonal geometry (i.e. ∠PCuP, ∠PCuO, and ∠OCO = 120°) unless stated otherwise. Note that the X-ray values are indeed 120 ± 5°. To simplify the calculations (limitations in the size of the molecules handled by the program), the dppm ligands were replaced by two PH_3 groups. Such a procedure is standard. Similarly, $^{-}O_2CCH_3$ was replaced by $^{-}O_2CH$. The reported density functional theoretical calculations (DFT) were all carried out by utilizing the program ADF version 1.1.3, which was developed by Baerends et al.[11] and vectorized by Raveneck.[12] The computations were used primarily for geometry optimization purposes. The numerical integration procedure applied for the calculations was developed by te Velde et al.[13] The geometry optimization procedure was based on the method developed by Versluis and Ziegler.[14] The electronic configurations of the molecular systems were described by an uncontracted double-ζ basis set[15] on copper for 3s, 3p, and 4s and triple-ζ for 4d. Double-ζ STO basis sets[16] were used for phosphorus (3s, 3p), oxygen (2s, 2p), carbon (2s, 2p), and hydrogen (1s), augmented with a single 3d polarization function, except for hydrogen, where a 2p function was used. Polarization functions were not used for copper. The $1s^22s^22p^6$ configuration on copper, the $1s^22s^2$ configuration on phosphorus, and the $1s^2$ configuration on oxygen and carbon were assigned to the core and treated by the frozen-core approximation.[11] A set of auxiliary[17] s, p, d, f, and g STO functions, centered on all nuclei, was used in order to fit the molecular density and present Coulomb and exchange potentials accurately in each SCF cycle. Energy differences were calculated by including the local exchange-correlation potential of Vosko et al.[18] No nonlocal exchange and nonlocal correlation corrections were made for the geometry optimization.

Crystallography. The crystalline material belongs to the triclinic system, space group $P\bar{1}$, with cell parameter values of a = 11.572(2) Å, b = 12.552(2) Å, and c = 19.543(3) Å, α = 85.274(12)°, β = 82.108(11)°, and γ = 68.950(12)°. Intensity data were collected at 293 K (20 °C) on an Enraf-Nonius CAD-4 automatic diffractometer using Mo Kα radiation. Table 1 provides crystallographic and data collection details. The NRCCAD[19] programs were used for centering, indexing, and data collection. The unit cell dimensions were obtained by least-squares fits of 24 centered reflections in the range 36° ≤ 2θ ≤ 40°. During data collection, the intensities of two standard reflections were monitored every 60 min. No significant decay was observed. An absorption correction based on ψ scan measurements of nine azimutal reflections was applied to the data. The minimum and maximum transmission factors were 0.6698 and 0.7999, respectively. The structure was solved by the application of direct methods using the NRCVAX[20] program and refined by least-squares procedures using SHELXL-93.[21] An isotropic extinction coefficient was included in the refinement to account for secondary extinction effects but a value of 0.0000(4) remained.[22] The atomic scattering factors in stored SHELXL-93 are from the *International Tables*, Vol. C, Tables 4.2.6.8 and 6.1.1.4. Hydrogen atoms were geometrically placed at idealized positions and not refined. At convergence, the final discrepancy indices[25] were S = 0.991, R = 0.0549, and R_{w2} = 0.1292. Refinement was based on F^2 for all reflections, weighted R factors R_w and all goodness of fits S were based on F^2, and conventional R factors R were based on F, with F set to zero for negative F^2. The observed criterion of $F^2 > 2\sigma(F^2)$ was used only for calculating observed R factors and was not relevant to the choice of reflections for refinement. R factors based on F^2 are statistically about twice as large as those based on F, and R factors based on all data are larger. The residual positive and negative electron densities in the final maps were 0.731 and −0.505 e/Å^3 and were located in the vicinity of the Cu atom. All esd's (except the esd's in the dihedral angle between two least-squares planes) were estimated using the full covariance matrix. The cell esd's were taken into account individually in the estimation of esd's in distances, angles, and torsion angles; correlation between esd's in cell parameters were only used when they were defined by crystal symmetry. The experimental density was not measured.

Table 1. Crystallographic Data for $[Cu_2(dppm)_2(O_2CCH_3)]BF_4\cdot(CH_3)_2CO$

empirical formula	$Cu_2P_4BC_{55}F_4O_3H_{53}$	γ, deg	68.950(12)
fw	1099.83	V, Å^3	2622.3(6)
space group	$P\bar{1}$	Z	2
T, °C	20(2)	λ, Å	0.710 73
a, Å	11.572(2)	ρ_{calcd}, g cm^{-3}	1.393
b, Å	12.552(2)	μ, cm^{-1}	9.9
c, Å	19.543(3)	R^a	0.0549
α, deg	85.274(12)	$R_w{}^b$	0.1292
β, deg	82.108(11)		

^{a} $R = \sum(F_o - F_c)/\sum F_o$. ^{b} $R_w = [\sum w(F_o - F_c)^2/\sum(wF_o^2)]^{1/2}$. $w = (\sigma^2(F) + 0.0002F^2)^{-1}$.

Results and Discussion

1. X-ray Structure. $[Cu_2(dppm)_2(O_2CCH_3)]BF_4$ is obtained in 92% chemical yield via the direct reaction between the cluster compound $[Cu_3(dppm)_3OH](BF_4)_2$ and CH_3CO_2Na in excess over a period of a few days. Crystals suitable for X-ray crystallography are easily obtained from acetone. The crystal data and the atomic coordinates are provided in Tables 1 and 2, respectively. The molecular structure exhibits two Cu(I) atoms bridged by two dppm ligands and one $CH_3CO_2^-$ ligand in a face-to-face fashion. The two metals are tricoordinated in a quasi-planar triangular fashion (Figure 1). This structure is closely related to other $d^{10}-d^{10}$ species such as the $M_2(dppm)_3$ complexes (M = Pd, Pt),[24] $Au_2(dmpm)_3^{2+}$ (dmpm = $((CH_3)_2P)_2CH_2$),[25] and $Cu_2(dppm)_2(ONC_5H_3CH_3)^+$ ($ONC_5H_3CH_3$ = 6-methylpyridin-2-olato). In the $Cu_2(dppm)_2(O_2CCH_3)^+$ case, the

(9) (a) Hoffmann, R.; Lipscomb, W. M. *J. Chem. Phys.* **1962**, *36*, 2179. (b) Hoffmann, R.; Lipscomb, W. M. *J. Chem. Phys.* **1962**, *37*, 2872. (c) Hoffmann, R. *J. Chem. Phys.* **1963**, *39*, 1397.
(10) (a) Ammeter, J. H.; Burgi, H. B.; Thibeault, J. C.; Hoffmann, R. *J. Am. Chem. Soc.* **1978**, *100*, 3686. (b) Summerville, R. H.; Hoffmann, R. *J. Am. Chem. Soc.* **1976**, *98*, 7240. (c) Hay, P. J.; Thibeault, J. P.; Hoffmann, R. *J. Am. Chem. Soc.* **1975**, *97*, 4884.
(11) (a) Baerends, E. J.; Ellis, D. E.; Ros, P. *Chem. Phys.* **1973**, *2*, 41. (b) Baerends, E. J. Ph.D. Thesis, Vrije Universiteit, Amsterdam, 1975.
(12) Raveneck, W. In *Algorithms and Applications on Vector and Parallel Computers*; Rigie, H. J. J., Dekker, Th. J., van de Vorst, H. A., Eds.; Elsevier: Amsterdam, 1987.
(13) Boerrigter, P. M.; te Velde, G.; Baerends, E. J. *Int. J. Quantum Chem.* **1988**, *33*, 87.
(14) Versluis, L.; Ziegler, T. *J. Chem. Phys.* **1988**, *88*, 322.
(15) (a) Snijders, G. J.; Baerends, E. J.; Vernooijs, P. *At. Nucl. Data Tables* **1982**, *26*, 483. (b) Vernooijs, P.; Snijders, G. J.; Baerends, E. J. *Slater Type Basis Functions for the Whole Periodic System: Internal Report*; Free University of Amsterdam: Amsterdam, 1981.
(16) (a) Noodleman, L.; Norman, J. G. *J. Chem. Phys.* **1979**, *70*, 4903. (b) Noodleman, L. *J. Chem. Phys.* **1981**, *74*, 5737. (c) Noodleman, L.; Baerends, E. J. *J. Am. Chem. Soc.* **1984**, *106*, 2316.
(17) Krijn, J.; Baerends, E. J. *Fit Functions in the HFS-method: Internal Report* (in Dutch); Free University of Amsterdam: Amsterdam, 1984.
(18) Vosko, S. D.; Wilk, L.; Nusair, M. *Can. J. Phys.* **1990**, *58*, 1200.
(19) LePage, Y.; White, P. S. Gabe, E. J. NRCCAD: An Enhanced CAD-4 Control Program. *Proceedings of the American Crystallographic Association Meeting*, Hamilton, 1986; Abstract PA23.
(20) Gabe, E. J.; LePage, Y.; Charland, J.-P.; Lee, F. L.; White, P. S. *J. Appl. Crystallogr.* **1989**, *22*, 384.
(21) Sheldrick, G. M. SHELXL-93. University of Göttingen, Germany, 1993.
(22) $F_c^* = kF_c[1 + 0.001F_c^2\lambda^3/\sin(2\theta)]^{-1/4}$.
(23) The weighting scheme used was $w = 1/[\sigma^2(F_o^2) + (0.084P)^2]$ where $P = (F_o^2 + 2F_c^2)/3$.
(24) (a) Manojlovic-Muir, L. J.; Muir, K. W. *J. Chem. Soc., Chem. Commun.* **1982**, 1155. (b) Manojlovic-Muir, L. J.; Muir, K. W.; Grossel, M. C.; Brown, M. P.; Nelson, C. D.; Yavani, A.; Kallas, E.; Moulding, R. P.; Seddon, K. R. *J. Chem. Soc., Dalton Trans.* **1985**, 1955. (c) Kirss, R. V.; Eisenberg, R. *Inorg. Chem.* **1989**, *28*, 3372.
(25) Bensch, W.; Prelati, M.; Ludwig, W. *J. Chem. Soc., Chem. Commun.* **1986**, 1762.

Table 2. Atomic Coordinates ($\times 10^4$) and Equivalent Isotropic Displacement Parameters ($Å^2 \times 10^3$)[a] for **1**

	x	*y*	*z*	*U*(eq)
Cu(1)	705(1)	2250(1)	2529(1)	48(1)
Cu(2)	2595(1)	3165(1)	2410(1)	46(1)
P(1)	−22(1)	3108(1)	1537(1)	47(1)
P(2)	2163(1)	3932(1)	1356(1)	46(1)
P(3)	2172(1)	4035(1)	3418(1)	41(1)
P(4)	245(1)	2882(1)	3618(1)	39(1)
O(2)	3694(4)	1527(4)	2449(2)	64(1)
O(3)	2215(4)	791(3)	2420(2)	65(1)
C(1)	522(5)	4291(5)	1254(3)	52(2)
C(2)	578(5)	4168(4)	3761(3)	44(1)
C(6)	3314(7)	716(6)	2424(3)	59(2)
C(7)	4304(7)	−468(6)	2419(4)	99(3)
C(11)	−1708(5)	3721(6)	1543(3)	54(2)
C(12)	−2394(6)	4837(6)	1688(4)	74(2)
C(13)	−3677(7)	5239(8)	1740(4)	94(3)
C(14)	−4315(7)	4548(10)	1657(4)	100(3)
C(15)	−3662(8)	3452(10)	1505(5)	114(3)
C(16)	−2345(7)	3018(7)	1439(4)	90(2)
C(21)	439(5)	2216(5)	787(3)	51(2)
C(22)	1249(6)	1123(6)	841(3)	67(2)
C(23)	1625(8)	444(7)	264(4)	100(3)
C(24)	1195(9)	857(9)	−352(4)	111(3)
C(25)	393(8)	1941(8)	−408(4)	98(3)
C(26)	18(7)	2634(6)	157(3)	72(2)
C(31)	3044(5)	3016(5)	646(3)	52(2)
C(32)	4114(6)	2141(5)	773(3)	60(2)
C(33)	4844(7)	1423(6)	248(4)	81(2)
C(34)	4478(9)	1578(7)	−396(4)	93(3)
C(35)	3417(9)	2452(8)	−537(4)	94(3)
C(36)	2694(6)	3188(6)	−18(3)	74(2)
C(41)	2449(5)	5267(5)	1140(3)	51(2)
C(42)	3202(6)	5438(6)	569(3)	64(2)
C(43)	3454(7)	6434(8)	487(4)	89(2)
C(44)	2968(8)	7256(6)	968(5)	84(2)
C(45)	2195(7)	7105(6)	1531(4)	81(2)
C(46)	1924(6)	6124(6)	1621(3)	65(2)
C(51)	2214(5)	5475(5)	3418(3)	45(1)
C(52)	3351(5)	5591(5)	3239(3)	62(2)
C(53)	3459(6)	6655(6)	3187(4)	68(2)
C(54)	2422(7)	7612(5)	3317(3)	66(2)
C(55)	1278(6)	7517(6)	3488(4)	73(2)
C(56)	1174(5)	6440(5)	3538(3)	59(2)
C(61)	3070(5)	3299(5)	4121(3)	44(1)
C(62)	3929(5)	2217(5)	4028(3)	60(2)
C(63)	4559(6)	1601(6)	4577(4)	79(2)
C(64)	4303(8)	2101(8)	5209(4)	85(2)
C(65)	3480(8)	3166(8)	5304(3)	77(2)
C(66)	2871(6)	3791(5)	4760(3)	61(2)
C(71)	−1414(5)	3341(4)	3917(3)	41(1)
C(72)	−1918(5)	2987(5)	4536(3)	58(2)
C(73)	−3180(6)	3353(6)	4710(3)	71(2)
C(74)	−3974(5)	4074(6)	4283(4)	67(2)
C(75)	−3482(6)	4460(7)	3680(4)	82(2)
C(76)	−2221(6)	4089(6)	3500(3)	69(2)
C(81)	960(5)	1818(5)	4266(3)	41(1)
C(82)	1327(6)	696(5)	4110(3)	63(2)
C(83)	1819(8)	−177(5)	4589(4)	86(2)
C(84)	1985(6)	95(6)	5222(3)	75(2)
C(85)	1633(6)	1204(6)	5392(3)	58(2)
C(86)	1110(5)	2073(5)	4914(3)	48(1)
B	7985(11)	7170(9)	2649(5)	90(3)
F(1)	8928(5)	6141(5)	2626(3)	154(2)
F(2)	8088(7)	7824(6)	3106(3)	176(3)
F(3)	7944(9)	7640(6)	2032(3)	206(4)
F(4)	6857(6)	7002(5)	2786(4)	161(2)
O(1)	9216(7)	1258(6)	2819(4)	142(3)
C(3)	8670(10)	703(8)	2657(4)	99(3)
C(4)	7300(10)	935(11)	2902(6)	183(6)
C(5)	9237(16)	−178(10)	2185(6)	236(8)

[a] *U*(eq) is defined as one-third of the trace of the orthogonalized $\mathbf{U}_{ij}$ tensor.

orientation of the methylene groups indicates a quasi-C_{2v} local symmetry for the $Cu_2(PCP)_2(OCO)$ skeleton. The *r*(CuO) distances (2.029(4) and 1.993(4) Å) are very close to the sum of the covalent radii (r_{cov} = 1.28 and 0.70 Å for Cu and O, respectively)[26] and far from the sum of the ionic radii (r_{ion} = 0.91 (Cu^+) and 1.26 Å (O^{2-})).[26] These *r*(CuO) data compare favorably to those for other carboxylate complexes of Cu(I). The PCuP and PCuO angles average 129.7(0.8) and 114.8(1.7)°, respectively. The quasi-triangular planes are not perfectly parallel as the average PCuCu angle is ~93°.

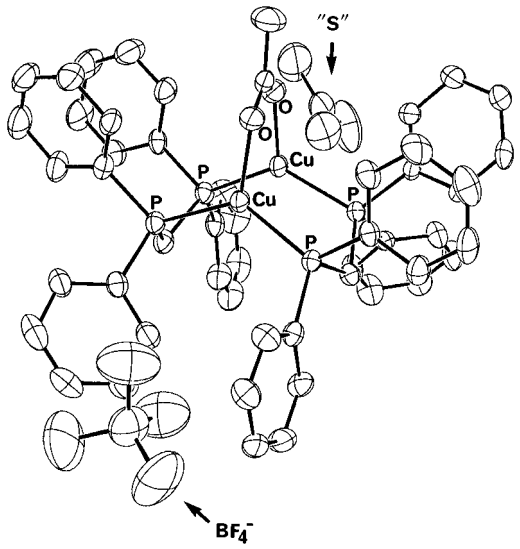

Figure 1. X-ray structure of $[Cu_2(dppm)_2(O_2CCH_3)]BF_4 \cdot (CH_3)_2CO$. The ORTEP diagram is shown with 50% probability ellipsoids. The H atoms are omitted for clarity. Note that "S" = $(CH_3)_2CO$. The atom numbering is provided in the Supporting Information.

There are no formal Cu−Cu bonds, but weak Cu···Cu interactions are suspected (*r*(Cu···Cu) = 2.7883(11) Å) as the measured distance lies barely under the sum of the van der Waals radii (r_{vdW}(Cu) = 1.40 Å). Evidence for M···M interactions for distances exceeding $2r_{vdW}$ has been provided by Raman and electronic spectroscopy for many $d^{10}-d^{10}$ species (M = Pd, Pt, Ag, Au, Hg).[27] For molecules carrying the "$Cu_2(dppm)_2$" unit, this distance is among the shortest observed. The only exception is $Cu_2(dppm)_2(ONC_5H_3CH_3)^+$, where *r*(Cu···Cu) = 2.679(6) Å. Rigidity is suspected to be at the origin of this behavior as the three shortest Cu···Cu distances are found in $Cu_3(dppm\text{-}H)_3$(dppm-H = $((C_6H_5)_2P)CH^-$; 2.836(4) Å),[26] $Cu_2(dppm)_2(O_2CCH_3)^+$ (2.7883(11) Å), and $Cu_2(dppm)_2(ONC_5H_3CH_3)^+$ (2.679(6) Å).[29] Relevant to this work, the X-ray structure of the copper(I) acetate complex ($Cu_4(O_2CCH_3)_4$) reveals the dimerization of two $Cu_2(O_2CCH_3)_2$ units where the Cu···Cu distance is very short 2.557(2) Å.[30] Selected distances and angles are presented in Table 3.

2. Metal−Metal Interactions. The M_2 interactions have been addressed by FT-Raman spectroscopy via the measurements of $\nu(M_2)$. The strategy of assignment is based upon the comparison with literature data for related complexes (Table 4) taking into account the M_2 bond lengths or separations and

(26) Cotton, F. A.; Wilkinson, G.; Gauss, P. L. *Basic Inorganic Chemistry*, 3rd ed.; Wiley: Toronto, 1995; p 61.
(27) (a) Perreault, D.; Drouin, M.; Michel, A.; Miskowski, V. M.; Schaefer, W. P.; Harvey, P. D. *Inorg. Chem.* **1992**, *32*, 695. (b) Perreault, D.; Drouin, M.; Michel, A.; Harvey, P. D. *Inorg. Chem.* **1993**, *32*, 1903. (c) Harvey, P. D.; Truong, K. D.; Aye, K. T.; Bandrauk, A. D. *Inorg. Chem.* **1994**, *33*, 3424. (d) Harvey, P. D.; Aye, K. T.; Isabel, E.; Hierso, K.; Lognot, I.; Mugnier, Y.; Rochon, F. *Inorg. Chem.* **1994**, *33*, 5981. (e) Harvey, P. D. *Coord. Chem. Rev.* **1996**, *153*, 175.
(28) Camus, A.; Marsich, N.; Nardin, G.; Randaccio, L. *J. Organomet. Chem.* **1973**, *60*, C39.
(29) Diez, J.; Gamasa, P.; Gimeno, J.; Manfranchi, M.; Tiripicchio, A. *J. Chem. Soc., Dalton Trans.* **1990**, 1027.
(30) Ogura, T.; Mounts, R. D.; Fernando, Q. *J. Am. Chem. Soc.* **1973**, *95*, 949.

Table 3. Selected Distances (Å) and Angles (deg)[a]

Cu(1)−Cu(2)	2.7883(11)	Cu(1)−P(4)	2.258(2)
Cu(1)−O(3)	2.029(4)	Cu(2)−P(3)	2.241(2)
Cu(2)−O(2)	1.993(4)	Cu(2)−P(2)	2.243(2)
Cu(1)−P(1)	2.254(2)		
P(1)−Cu(1)−P(4)	130.56(6)	O(3)−Cu(1)−Cu(2)	80.40(14)
P(3)−Cu(2)−P(2)	128.87(6)	P(1)−Cu(1)−Cu(2)	93.74(5)
O(3)−Cu(1)−P(1)	115.48(12)	P(4)−Cu(1)−Cu(2)	85.47(4)
O(3)−Cu(1)−P(4)	113.08(12)	O(2)−Cu(2)−Cu(1)	83.19(14)
O(2)−Cu(2)−P(3)	114.41(12)	P(3)−Cu(2)−Cu(1)	100.65(5)
O(2)−Cu(2)−P(2)	116.19(12)	P(2)−Cu(2)−Cu(1)	92.10(5)

[a] Atom labeling can be found in the Supporting Information.

Table 4. Structural and Spectroscopic Data for Cu_2 Compounds and Other Related $d^{10}-d^{10}$ Species

	$r(M_2)$, Å	$\nu(M_2)$, cm^{-1}	$F(M_2)$, mdyn $Å^{-1}$ [a]
$[Cu_2(dppm)_2(CH_3CO_2)]BF_4$	2.788(1)[b]	87.7[b]	0.20[b]
$Cu_2(O_2CCH_3)_4$	2.64(1)[c]	177[d]	0.49
$Cu_2(A\ ^1\pi_u)$	2.5584[e]	191.9[e]	0.91
$Cu_2(B\ ^1\Sigma_u^+)$	2.3276[e]	242.15[e]	1.45
$Cu_2(X\ ^1\Sigma_g^+)$	2.2197[e]	264.55[e]	1.72
$[Ag_2(dppm)_3](PF_6)_2$	3.10(1)[f]	76[g]	0.18[g]
$[Ag_2(dmpm)_2](PF_6)_2$	3.041(1)[h]	76[g]	0.18[g]
$Ag_2(O_2CCF_3)_2$	2.967(3)[i]	80[j]	0.20[g]
$[Au_2(dmpm)_3](PF_6)_2$	3.045(5)[k]	68[j]	0.27[j]
$[Au_2(dmpm)_2](PF_6)_2$	3.044(i)[j]	69[j]	0.28[j]

[a] Diatomic approximation, unless stated otherwise [b] This work. [c] From: Van Niekerk, J. N.; Schoening, F. R. L. *Acta Crystallogr.* **1953**, *6*, 227. [d] See footnote 34. [e] From: Huber, K. P.; Herzberg, G. *Molecular Spectra and Molecular Structure Constants of Diatomic Molecules*; Van Nostrand: New York, 1979. [f] Average values for various $Ag_2(dppm)_2^{2+}$ species were taken from: Ho, D. M.; Bau, R. *Inorg. Chem.* **1983**, *22*, 4073. [g] From: Perreault, D.; Drouin, M.; Michel, A.; Miskowski, V. M.; Schaefer, W. P.; Harvey, P. D. *Inorg. Chem.* **1992**, *32*, 695. [h] From: Stendel, R. *Z. Naturforsch.* **1975**, *30B*, 281. [i] From: Griffin, R. G.; Ellett, J. D., Jr.; Mehring, M.; Bullitt, J. G.; Waugh, J. S. *J. Chem. Phys.* **1972**, *57*, 2147. [j] From: Perreault, D.; Drouin, M.; Michel, A.; Harvey, P. D. *Inorg. Chem.* **1993**, *32*, 1903. [k] From: Bensch, W.; Prelati, M.; Ludwig, W. *J. Chem. Soc., Chem Commun.* **1986**, 1762.

the commonly encountered high intensity of the $\nu(M_2)$ modes.[31−33] During the course of this investigation, the $\nu(Cu_2)$ peak of the related complex $Cu_2(O_2CCH_3)_4$ has been assigned (i.e. 177 cm^{-1}).[34] The FT-Raman spectrum of the $Cu_2(dppm)_2(O_2CCH_3)^+$ complex (Figure 2) exhibits only one intense feature

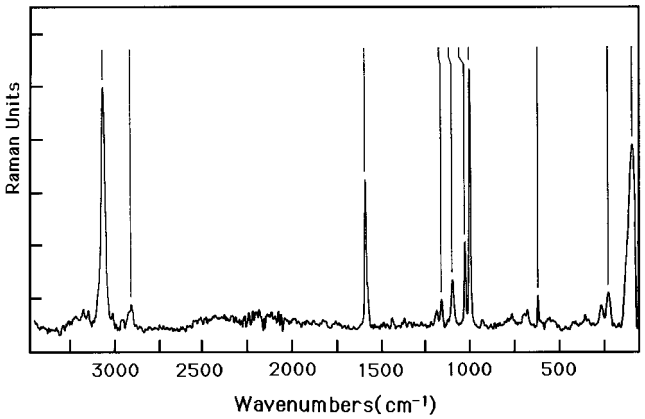

Figure 2. FT-Raman spectrum of solid $[Cu_2(dppm)_2(O_2CCH_3)]BF_4$ at room temperature. Experimental conditions: 300 scans, 4 cm^{-1} resolution, baseline corrected. The vertical lines mark the 3056.4, 2901.6, 1586.8, 1159.8, 1098.8, 1028.5, 1000.9, 618.2, 223.3, and 87.7 cm^{-1} peaks.

in the low-frequency region at 87.7 cm^{-1}, which is readily assigned to $\nu(Cu_2)$. This value compares very favorably to that of other related Ag^I complexes (Table 4). The Cu_2 force constant, $F(Cu_2)$, is 0.20 mdyn $Å^{-1}$ and indicates that the Cu_2 interactions are very weak. The $F(Cu_2)$ value for the singly bonded Cu_2 ($^1\Sigma_g^+$) molecule is 1.72 mdyn $Å^{-1}$. We find a reasonable correlation among $r(Cu_2)$, $\nu(Cu_2)$, and $F(Cu_2)$ (Table 4).

3. Theoretical Calculations. EHMO calculations were performed to determine the nature of the frontier orbitals. MO representations were plotted by using CACAO software. The computations were performed for two model complexes: $Cu_2(PH_3)_4(O_2CH)^+$ and $Cu_2(PH_2(C_6H_5))_4(O_2CCH_3)^+$. The first complex is simple and is designed to address MO's potentially capable of generating $d\sigma^* \rightarrow p\sigma$, d → s, and Cu → "$O_2C$" excited states. The second model complex is closer to the X-ray structure, where the phenyl groups are incorporated onto the phosphines, and addresses the charge transfers between the Cu centers and the phenyl groups and the intraligand transitions ($\pi \rightarrow \pi^*$). In order to avoid unnecessary complications of the MO diagram, and due to the limitation in size of the computations, only four phenyl groups were used. Two were placed parallel to the CuP_2O planes, and two pointed downward, somewhat similar to those in the X-ray structure (Figure 1). The molecular axis along the C−H or C−CH_3 bonds was the *z* axis, while the Cu···Cu interactions occurred along the *x* axis according to the computations. However, these interactions took place via the d_{z^2} and p_z Cu orbitals perpendicular to the CuP_2O planes. The MO analysis was performed as such.

The MO ordering for the frontier MO's of $Cu_2(PH_3)_4(O_2CH)^+$ is shown in Figure 3 , and the atomic contributions are provided in Table 5. The three lowest unoccupied MO's (LUMO+2, LUMO+1, and LUMO) are the Cu_2 $p\sigma^*$ and $p\sigma$ orbitals and the π^* system of the HCO_2 fragment, respectively. These are located at −5.198, −6.975, and −8.667 eV, respectively. The LUMO is largely composed of the (out-of-plane) C p_y orbital (76%). The computed HOMO is located 4.13 eV below the LUMO. This MO exhibits three distinct fragments. The first fragment is the $d\delta^*$ MO centered on Cu_2 and arising from the $d_{xy}-d_{xy}$ interactions. The second fragment originates from the four P p_y atomic orbitals, together contributing to 24% of the MO. The Cu−P interactions are antibonding and are described as σ^*(CuP) in Table 5. The third fragment is located in the O p_y orbitals of the HCO_2 moieties and contributes to only 4% of the MO. This fragment is the nonbonding $-CO_2$ π system. The addition of this contribution to the HOMO slightly raises the energy of this MO. HOMO-1 is located ∼0.4

(31) Nakamoto, K. *Infrared and Raman Spectra of Inorganic and Coordination Compounds*, 4th ed.; Wiley: Toronto, 1986.

(32) Because of the white coloration of the compound, resonance Raman spectroscopy could not be employed here as a means of selectively enhancing the $\nu(Cu_2)$ peak. Furthermore, the nature of the lowest energy bands is not $d\sigma^* \rightarrow p\sigma$ but rather is MLCT where L = CH_3CO_2 (see text). Thus, the resonance enhancement would not affect $\nu(Cu_2)$ in this case. In addition, a polarization study could not be performed either, as the low-frequency region becomes hidden under a large Raleigh scattering band when the compound is dissolved in solution.

(33) A list of proposed assignments is provided in the Supporting Information.

(34) (a) The Raman spectrum of the solid $Cu_2(O_2CCH_3)_4$ complex has been reported by San Filippo and Sniadoch,[34b] but the $\nu(Cu_2)$ peak has not been assigned. For comparison with the $Cu_2(dppm)_2(O_2CCH_3)^+$ complex, we have located $\nu(Cu_2)$ in this case. The reported Raman peaks below 500 cm^{-1} are 325 vs, 250 m, 230 m, 177 m, 110 m, and 100 cm^{-1} s. On the basis of the Cu_2(g) data (Table 4), $\nu(Cu_2)$ must be located below 200 cm^{-1}. By comparison with known M_2 complexes where M = a 3d metal with similar M_2 separations ($Mn_2(CO)_{10}$, $r(Mn_2)$ = 2.895 Å,[34c] $\nu(Mn_2)$ = 160 cm^{-1};[34d] $Fe_2(CO)_6S_2$, $r(Fe_2)$ = 2.55 Å,[34e] $\nu(Fe_2)$ = 195 cm^{-1} [34f]), the only reasonable candidate for $\nu(Cu_2)$ in $Cu_2(O_2CCH_3)_4$ is the 177 cm^{-1} peak. (b) San Filippo, J., Jr.; Sniadoch, H. J. *Inorg. Chem.* **1973**, *12*, 2326. (c) Churchill, M. R.; Amoh, K. N.; Wasserman, H. J. *Inorg. Chem.* **1981**, *20*, 1609. (d) Svec, H. J.; Junk, G. A. *J. Am. Chem. Soc.* **1967**, *89*, 2836. (e) Wei, C. W.; Dahl, L. F. *Inorg. Chem.* **1965**, *4*, 1. (f) Kubas, G. J.; Spiro, T. G. *Inorg. Chem.* **1973**, *12*, 1797.

Table 5. Atomic Contributions (EHMO) to the Frontier Orbital of the Model Complex $Cu_2(PH_3)_4(O_2CH)^+$ [a]

		Cu %								P %				O %			C %	
MO no.	*E*, eV	$d_{x^2-y^2}$	d_{z^2}	d_{xy}	d_{yz}	d_{xz}	p_x	p_y	p_z	s	p_x	p_y	p_z	p_x	p_y	p_z	p_y	assignt
22($11b_1$)	−5.198						12		76	4								pσ*
23($12a_1$)	−6.975								86									pσ
24($8b_2$)	−8.667														24		76	π*(HCO_2); LUMO
25($7a_2$)	−12.797			48				14				24			4			dδ* + σ*(CuP) + n(O); HOMO
26($7b_2$)	−13.221			66				10				16						dδ + σ*(CuP)
27($11a_1$)	−13.300	52	8			4	4							22				dδ* + σ(CuO)
28($9b_1$)	−13.336	66	6				4							14				dδ + σ*(CuO)
29($9b_1$)	−13.627	10	82							4								dσ*
30($8b_1$)	−13.768	6				78										12		dπ*
31($10a_1$)	−13.829			4	90													dπ*
32($10a_1$)	−13.992	8				86												dπ
33($6b_2$)	−14.049				98													dπ
34($9a_1$)	−14.168	10	86							4								dσ

[a] Contributions of less than 1% are not indicated. The MO symmetry labels refer to the *z* axis parallel to the C−H bond and the *x* axis along the Cu···Cu interactions. The d_{z^2} Cu orbital is perpendicular to the CuL_3 plane also along the Cu···Cu interactions.

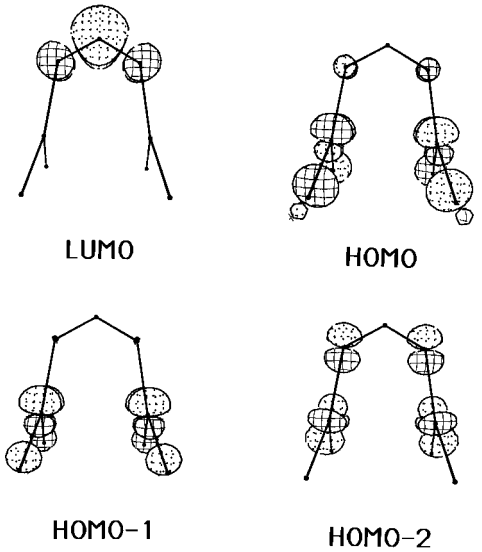

Figure 3. MO diagrams of the frontier orbitals (LUMO, HOMO, HOMO-1, HOMO-2) for the model complex $Cu_2(PH_3)_4(O_2CCH)^+$.

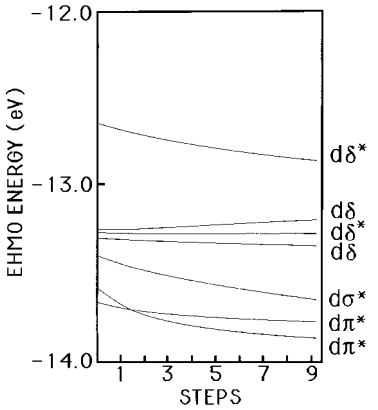

Figure 4. EHMO energies of the seven highest occupied molecular orbitals for the model complex $Cu_2(PH_3)_4(O_2CCH)^+$ as a function of the Cu···Cu separation between 2.585 and 2.865 Å. Each step represents a 0.035 Å increment.

eV below and is the dδ + σ*(CuP) MO, also via the $d_{xy}-d_{xy}$ interactions. The atomic contributions are somewhat similar to those of the HOMO, but no O p_y contribution is computed. HOMO-2 and HOMO-3 are the dδ* and dδ systems, respectively, arising from the $d_{x^2-y^2}-d_{x^2-y^2}$ interactions. Minor contributions from the in-plane O p_x orbitals are also computed. These Cu−O interactions are antibonding. Below these MO's follow the dσ* ($d_{z^2}-d_{z^2}$), dπ* ($d_{xz}-d_{xz}$), dπ* ($d_{yz}-d_{yz}$), dπ ($d_{xz}-d_{xz}$), dπ ($d_{yz}-d_{yz}$), and dσ ($d_{z^2}-d_{z^2}$) MO's, all almost entirely located within the Cu_2 center. The calculated energy gaps for the pσ*−pσ, dδ*−dδ, dσ*−dσ, and dπ*−dπ MO's are 1.78 (p_z-p_z), 0.42 ($d_{xy}-d_{xy}$), 0.04 ($d_{x^2-y^2}-d_{x^2-y^2}$), 0.54 ($d_{z^2}-d_{z^2}$), 0.22 ($d_{xz}-d_{xz}$), and 0.22 eV ($d_{yz}-d_{yz}$) and indicate that weak Cu_2 interactions are taking place ($r(Cu_2)$ = 2.79 Å). Such Cu(I)−Cu(I) interactions have been theoretically predicted in many other polynuclear systems.[35]

The HOMO−LUMO energy gap is 4.13 eV, as already stated, and predicts that the lowest energy electronic band should be located in the 300 nm range. Experimentally this prediction is indeed verified (section below).

The MO ordering does not change for Cu_2 separations ranging from 2.585 to 2.865 Å, except for the dπ* MO's, which undergo crossing at $r(Cu_2)$ ∼2.62 Å (Figure 4). The filled MO's that undergo the largest energy changes are dσ*, dσ, and dδ* (HOMO) and the lowest energy dπ* ($6a_2$). For the dσ* and dσ orbitals, these energy changes are due to a simple change in $d_{z^2}-d_{z^2}$ orbital overlaps with the Cu_2 distance. For dδ* (HOMO), the gain in energy stabilization with the COCu angle is associated with a decrease in OCu orbital overlaps. These interactions are antibonding. Finally, for the dπ* ($6a_2$) orbital, the large energy change is also due to Cu $d_{yz}-d_{yz}$ overlaps. These interactions appear to be more sensitive than that of the $d_{xz}-d_{xz}$ overlap. Nonetheless, the main conclusion of these calculations is that the nature of the lowest energy excitation *is not predicted* to change in the 2.585−2.865 Å range if such an event would occur.

The MO diagram for the $Cu_2(PH_2(C_6H_5))_4(O_2CCH_3)^+$ model is as expected, significantly more complex. The LUMO and HOMO are essentially identical to those described above, with a minor difference for the LUMO. Some weak atomic contributions arising from the phenylphosphines (parallel to the CuP_2O planes) are computed (Figure 5). The HOMO−LUMO energy gap is 4.09 eV. About 0.1 eV above the LUMO lie eight quasi-degenerate phenyl π* MO's; these are located within ∼0.08 eV. Three of them include atomic contributions from the C atom of the CO_2 group. Below the HOMO (∼0.3 eV) lie also eight MO's associated with the phenyl π systems, which spread over a ∼0.14 eV range. These computations predict that the three electronic transitions should follow the following energetic order: Cu → acetate < Cu → phenylphosphines (π*)

(35) (a) Merz, K. M., Jr.; Hoffmann, R. *Inorg. Chem.* **1988**, *27*, 2120. (b) Jiang, Y.; Alvarez, S.; Hoffmann, R. *Inorg. Chem.* **1985**, *24*, 749. (c) Mehrotra, P. D.; Hoffmann, R. *Inorg. Chem.* **1978**, *17*, 2187. (d) Dedieu, A.; Hoffmann, R. *J. Am. Chem. Soc.* **1978**, *100*, 2074. (e) Cotton, F. A.; Feng, X.; Matusz, M.; Poli, R. *J. Am. Chem. Soc.* **1988**, *110*, 7077. (f) King, C.; Wang, J.-C.; Khan, Md. N. I.; Fackler, J. P., Jr. *Inorg. Chem.* **1989**, *28*, 2145.

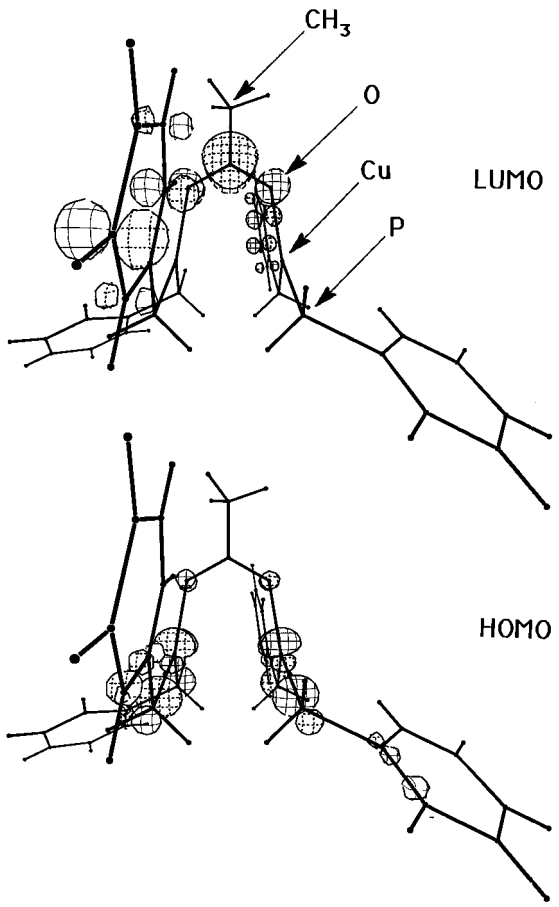

Figure 5. MO diagrams for the LUMO and HOMO of the $Cu_2(PH_2(C_6H_5))_4(O_2CCH_3)^+$ model compound.

< phenylphosphine intraligand $\pi \rightarrow \pi^*$. The closely placed LUMO and the upper MO's ($\Delta \sim 0.1$ eV) exhibit some degree of mixture according to the atomic contribution analysis. The lowest energy excited states are predicted to be delocalized (i.e. mixed) on both the acetate and phenylphosphines. Formal assignments for the luminescent states will be experimentally established below in the section discussing electronic spectra.

4. Geometry Optimizations. The ground state geometry optimizations were performed using the DFT to determine the role of the $CH_3CO_2^-$ bridging ligand in the Cu_2 separation. The $Cu_2(H_2PCH_2PH_2)_2(O_2CH)^+$ and $Cu_2(H_2PCH_2PH_2)_2^{2+}$ model complexes were used. The phenyl groups were not incorporated in these calculations. The electronic configurations computed according to DFT and EHMO theory are different. The DFT model predicts that the relative MO energy order is dδ* (HOMO) > dδ > dσ* > dπ* > dδ* > dπ* > dδ > dπ > dπ > dσ. Part of the reason for this is that 10 MO's are located only within ~1.5 eV and energy level inversions between the two models are likely to occur. Also, the DFT model predicts the presence of greater Cu_2 interactions for the same distance (i.e. ~2.8 Å). For instance, the computed dσ−dσ* energy gaps are 1.19 and 0.54 eV for the DFT and the EHMO models, respectively. This relation is also true for the dπ−dπ* and dδ−dδ* orbitals. Furthermore, the relative atomic contributions of the O atoms to the dδ and dδ* ($d_{x^2-y^2}$) orbitals are computed to be less important according to DFT, so that these orbitals are less destabilized. As a consequence, the increase in Cu_2 interactions causes the energies of the dσ* orbital and the two dπ* orbitals to increase and the slight change in relative atomic contributions causes the energies of the dδ and dδ* ($d_{x^2-y^2}$) orbitals to decrease, explaining the differences in the computed electronic configurations. The energies of the empty orbitals remain in the same order (pσ* > pσ > π*). More importantly for this work, both computations agree on the nature of the predicted lowest energy electronic transitions (MLCT; dδ* → π*(CH_3CO_2)). Of course, in the absence of phenyl groups on the phosphines, the effect of these substituents on the MO diagram cannot be predicted here.

Table 6. Comparison of the DFT-Optimized Geometries[a]

	$Cu_2(H_2PCH_2PH_2)^{2+}$ C_{2v}	$Cu_2(H_2PCH_2PH_2)_2(O_2CH)^+$	$Cu_2(dppm)_2(O_2CCH_3)^+$ X-ray average values
r(Cu_2)	2.565	2.520	2.788
r(CuO)		1.948	2.011
r(CuP)	2.212	2.214	2.249
r(CO)		1.254	1.247
r(PC)	1.806	1.835	1.830
∠(PCuP)	170.0	129.6	129.7
∠(OCuP)		114.8	114.8
∠(OCuCu)		86.0	81.8
∠(PCuCu)	95.0	95.7	85.7
∠(COCu)		120.3	124.5
∠(CPCu)	112.7	111.2	111.8

[a] Distances in angstroms; angles in degrees.

The results of the geometry optimizations for two model complexes $Cu_2(H_2PCH_2PH_2)_2^{2+}$ and $Cu_2(H_2PCH_2PH_2)_2(O_2CH)^+$ are presented in Table 6. The optimizations were performed using the C_{2v} point group where the CH_2 moieties were placed pointing downward as found crystallographically. The computed distances of single bonds (Cu−O, Cu−P, O−C, etc.) for the triply bridged species compare favorably with the X-ray data, as the differences between the two range from ~0.01 to 0.06 Å. At minimization, both model complexes predict strong Cu_2 interactions. In this case, DFT fails to accurately compute the Cu_2 separation, as it tends to overestimate the amplitude of the Cu_2 interactions. Nevertheless, only the trend in Cu_2 distances is of interest here when the RCO_2^- bridging ligand is removed from the complex. The calculated model complexes predict an increase in the Cu_2 distance in the absence of the carboxylate ligand. In other words, the small bite distance and the rigidity of the ligand promote Cu_2 interactions. However, these interactions are not great enough to bring the pσ orbital below the $\pi(O_2CH)$ orbital. So no low-energy dσ*−pσ electronic interaction is predicted by either theoretical model.

5. ^{1}H and ^{31}P NMR Data. The ^{1}H NMR spectra exhibit three types of H nuclei: 7.0−7.5 ppm = phenyl groups (br), 3.52 ppm = CH_2 (br), and 2.50 ppm = CH_3 (s), in CD_3CN. The dppm peaks are broad and can indicate the presence of ligand exchange,[36] ligand elimination,[36] or fluxionality processes.[37] Addition of free dppm to the solutions induces a gradual shift of the broad CH_2 signal (fwhm ~ 30 Hz) toward 3.18 ppm, while the CH_3 peak remains unchanged. No free-dppm peak appears (i.e. at ~2.96 ppm, triplet), indicating that the dppm is involved in a rapid exchange with the complex. Lowering the temperature of the pure complex from 313 to 213 K using acetone-d_6 as solvent induces the appearance of the free dppm at 2.93 ppm at ~263 K. The CH_2 peak shifts from 3.46 at 313 K to 3.84 ppm at 213 K (fwhm ~ 30 Hz), passing through a coalescence process (at ~253 K; fwhm ~ 100 Hz). During the experiment, the CH_3 signal remains sharp (fwhm is a few hertz) and shifts only slightly (by ~0.07 ppm). These two measurements indicate that the complex in solution is in equilibrium:

(36) Obendorf, D.; Probst, M.; Peringer, P.; Falk, H.; Muller, N. *J. Chem. Soc., Dalton Trans.* **1988**, 1709.
(37) The complex is diamagnetic, and the broadness of the ^{1}H NMR signals cannot be associated with paramagnetism.

Table 7. VT ^{31}P NMR Data

temp °C	temp K	δ, ppm (dominent peak)	fwhm, ppm	comments
25	298	−11.64	∼5	
19.5	292.5	−10.97	∼4.5	
9.5	282.5	−10.31	4.0	
−0.5	272.5	−9.55	3.2	appearance of a broad shoulder at 19.2 ppm
−10.5	262.5	−9.36	1.8	shoulder becomes a broad weak peak at ∼18.7 ppm
−20.5	252.5	−9.59	0.7	the weak peak becomes two peaks (−15.8 and −19.0 ppm)
−30.5	242.5	−9.89	0.3	the two weak peaks are well resolved (−15.3 and −19.3 ppm)
−40.5	232.5	−10.19	0.3	peaks at −16.0 and −19.0 ppm

$$Cu_2(dppm)_2(O_2CCH_3)^+ \leftrightarrows Cu_2(dppm)(O_2CCH_3)^+ + dppm \quad (1)$$

There are numerous examples of phosphine labilizations in d^{10} complexes in the literature.[38] The ^{31}P NMR spectrum exhibits only an intense and very broad signal centered at −10.64 ppm (vs H_3PO_4 in CD_3CN) at room temperature (i.e. 298 K). The fwhm is ∼5 ppm and also confirms the presence of chemical exchange. Upon cooling of the solutions, the spectra become better resolved (fwhm = 0.3 ppm for the dominent peak) and exhibit three ^{31}P signals (−10.2, −16.0, and −19.0 ppm). The dominant peak at 232.5 K is the −10.2 ppm signal and is associated with the $Cu_2(dpm)_2(O_2CCH_3)^+$ species. The two weaker signals (−19.0 ppm; free dppm) and (−16.0 ppm; $Cu_2(dppm)(O_2CCH_3)^+$) have somewhat similar intensities but are only about 10% as intense as the dominant peak. A description of the VT ^{31}P NMR measurements is provided in Table 7.

Additions of CH_3CO_2K to $Cu_2(dppm)_2(O_2CCH_3)^+$ in methanol-d_4 also induce a shift of the ^{1}H NMR CH_3 singlet (also fwhm ∼ 5 Hz) from 2.50 to 1.89 ppm (in excess) and a shift of the CH_2 signal from ∼3.4 to ∼3.3 ppm. Free $CH_3CO_2^-$ in methanol-d_4 exhibits a signal at ∼1.89 ppm and an fwhm of ∼1−2 Hz. This experiment is consistent with the following competitive equilibrium:

$$Cu_2(dppm)(O_2CCH_3)^+ + CH_3CO_2^- \leftrightarrows Cu_2(dppm)(O_2CCH_3)_2 \quad (2)$$

On the basis of the amount of $CH_3CO_2^-$ necessary to induce a significant shift in the δ values, it is anticipated that the equilibrium constant is not great. There has been no evidence for other species.

6. Electronic Spectra. The solid state spectra are discussed first. The beige compound is not luminescent at room temperature but exhibits a strong emission at 77 K. This emission is centered at ∼470 nm and exhibits no vibrational features. On the other hand, the solid state excitation spectrum at 77 K exhibits a poorly resolved band centered at ∼340 nm (Figure 6). The vibrational progression is located on the low-energy side of the band with a spacing of 523 ± 10 cm^{-1}. In the vibrational spectra, a medium-intensity IR band is observed at 516 cm^{-1} (Supporting Information), while in the FT-Raman spectrum, this band is presumably too weak to be seen in the noisy baseline (Figure 2). This vibrational frequency is too great to be assigned to an excited state $\nu(Cu_2)$ or $\nu(CuL)$[31,39] but is readily assigned to an intraligand vibrational mode.[40] At 9 K, some of the vibrational features increase in intensity and become somewhat slightly better resolved. The spacing remains the same.

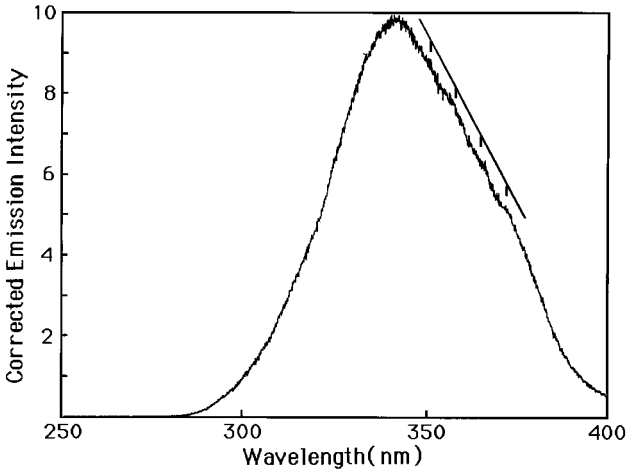

Figure 6. Solid state corrected excitation spectrum of $[Cu_2(dppm)_2(O_2CCH_3)]BF_4$ as a pressed pellet at 77 K. λ_{emi} = 470 nm. The marks at 352, 358, 365, and 372 nm, indicate the vibrational features.

The UV−visible spectrum of $Cu_2(dppm)_2(O_2CCH_3)^+$ in ethanol exhibits two intense absorptions at ∼305 (ϵ = 9880 M^{-1} cm^{-1} at 298 K in EtOH) and ∼265 nm (ϵ = 22900 M^{-1} cm^{-1} at 298 K in EtOH). There is no major spectral shift or change in bandwidth upon changing the temperature (298 and 77 K), indicating that the band associated with the dσ^* → pσ electronic transition does not occur within this spectral range.[41] At 77 K, the complex exhibits a strong emission in the 400−600 nm range (Figure 7). This luminescence band appears asymmetric where the λ_{max} is located at ∼440 nm, and a long tail extends all the way to 600 nm. On the basis of NMR data, two metal species must be present in solutions (i.e. $Cu_2(dppm)_2(O_2CCH_3)^+$ and $Cu_2(dppm)(O_2CCH_3)^+$). Indeed, time-resolved (TR) spectroscopy readily confirms the presence of two luminescing species using λ_{exc} = 330 nm (Figure 8). With short lifetimes (i.e. in the 50 μs delay time window), an asymmetric narrow emission appears at λ_{max} ∼435 nm. With longer delay times (i.e. at delay times ranging from 350 μs and 1 ms), another species of weaker intensity is evident at ∼480 nm. The comparison of the solid state datum (470 nm) and this 480 nm value suggests that this long-wavelength species is the $Cu_2(dppm)_2(O_2CCH_3)^+$ complex in solutions. To provide a formal assignment for the luminescence, the luminescence of free dppm has been investigated. From eq 1, three luminescent species are possible to explain the two emissions. Under the same experimental conditions as for the complex (i.e. λ_{exc} =

(38) (a) Mann, B. E.; Musco, A. *J. Chem. Soc., Dalton Trans.* **1975**, 1673. (b) Tolman, C. A.; Seidel, W. C.; Gerlach, D. H. *J. Am. Chem. Soc.* **1972**, *94*, 2669. (c) Ugo, R. *Coord. Chem. Rev.* **1968**, *3*, 319. (d) Birk, J. P.; Halpern, J.; Picard, A. L. *Inorg. Chem.* **1968**, *7*, 2672. (e) Ugo, R.; Cariti, F.; Monica, G. L. *J. Chem. Soc., Chem. Commun.* **1966**, 868. (f) Fitton, P.; McKeon, J. E. *J. Chem. Soc., Chem. Commun.* **1968**, 4. (g) Birk, J. P.; Halpern, J.; Picard, J. E. *J. Am. Chem. Soc.* **1968**, *90*, 4491. (h) Mann, B. E.; Musco, A. *J. Chem. Soc., Dalton Trans.* **1980**, 776.

(39) Clark, J. H. R.; Ferris, L. T. H. *Inorg. Chem.* **1981**, *20*, 2759.

(40) The IR spectra of dppm show no peak near 520 cm^{-1}, while a medium-strong IR band is observed at 525 cm^{-1} for solid CH_3CO_2Na.

(41) See numerous examples in the literature: (a) Harvey, P. D.; Gray, H. B. *J. Am. Chem. Soc.* **1988**, *110*, 2145. (b) Piché, D.; Harvey, P. D. *Can. J. Chem.* **1994**, *72*, 705. (c) Harvey, P. D.; Murtaza, Z. *Inorg. Chem.* **1993**, *32*, 4721.

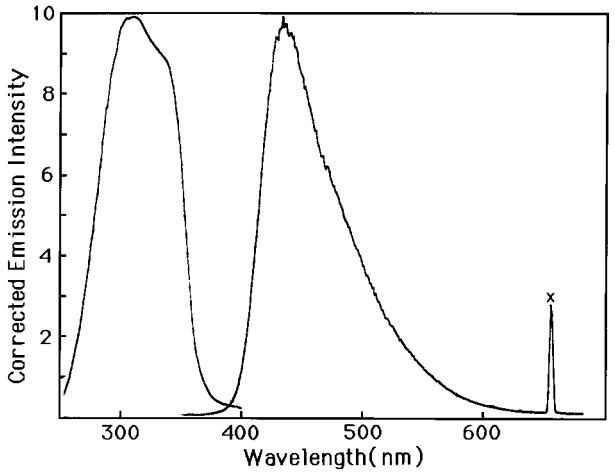

Figure 7. Corrected emission (right) and excitation spectra (left) of $[Cu_2(dppm)_2(O_2CCH_3)]BF_4$ in EtOH solution at 77 K. λ_{exc} for the emission spectrum = 330 nm, λ_{emi} for the excitation spectrum = 435 nm.

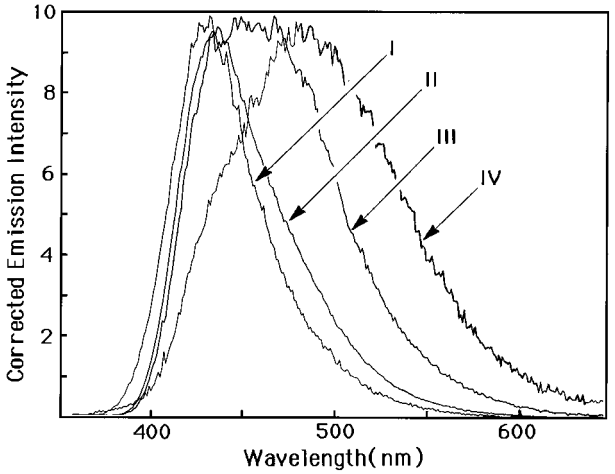

Figure 8. Time-resolved corrected emission spectra of $[Cu_2(dppm)_2(O_2CCH_3)]BF_4$ in EtOH at 77 K. Delay times: 0.001−10 μs (spectrum I), 10−50 μs (spectrum II), 50−350 ms (spectrum III), 350−1000 ms (spectrum IV). λ_{exc} = 330 nm.

330 nm, same solvents and concentrations), no emission was observed for dppm (i.e., the presence of free dppm does not interfere with the TR experiments). However, for comparison purposes, it is still possible to observe luminescence from dppm by using λ_{exc} = 300 nm. In this case, the luminescence is located at ∼445 nm and is very broad, expanding from ∼340 nm to way above 650 nm, and does not compare in any way to the spectra reported in Figure 8 (i.e. λ_{max} and bandwidth). This comparison allows one to definitely rule out the possibility of an intraligand dppm $\pi-\pi^*$ assignment. Further, it is unreasonable to assign to intraligand dppm $\pi \rightarrow \pi^*$ the observed luminescence in Figure 8, as the energy gap between the two emission maxima is on the order of 2200 cm^{-1}. The nature of the perturbation (addition of a dppm to the coordination sphere) does not justify such a shift. Upon addition of dppm (see eq 1), the intensity of the 480 nm band increases, indicating a shift of the equilibrium toward the tricoordinated Cu complex. The shape of the shorter wavelength emission band remains quasi-unaffected at very short delay times (from 0.001 to 50 μs), indicating that the longer emission band is weak and hidden under the tail of the stronger 435 nm band under these experimental conditions. The large Stokes shift (∼10 000 cm^{-1}; absorption = 350 nm (32 800 cm^{-1}), emission ≥ 435 nm (≥23 000 cm^{-1}) and the long emission lifetimes (>50 μs; discussed below) confirm that these emissions are both phosphorescence.

All emission lifetime (τ_e) solution data (measured at 77 K) exhibit a biexponential behavior as expected. The relative intensity (I_e) and τ_e are both medium dependent, presumably consistent with a solvent dependence on reaction 1. The data are as follows. 2-MeTHF: $I_1 = 0.63$, $\tau_1 = 50$ μs, $I_2 = 0.37$, $\tau_2 = 134$ μs. EtOH: $I_1 = 0.72$, $\tau_1 = 68$ μs; $I_2 = 0.28$, $\tau_2 = 234$ μs. Upon addition of free dppm to the solution, the I_1/I_2 ratios decrease, indicating the formation of $Cu_2(dppm)_2(O_2CCH_3)^+$ over $Cu_2(dppm)(O_2CCH_3)^+$. Since the emission quantum yields for both species are unknown, no further analysis, such as the evaluation of the radiative and nonradiative rate constants, can be done under these experimental conditions.

The $Cu_2(dppm)_2(O_2CC_6H_5)^+$ complex was also investigated to experimentally determine the nature of the lowest energy emissive excited states. On the basis of the EHMO calculations, a mixed Cu → phenylphosphine/acetate charge transfer lowest energy excited state is predicted (the intraligand dppm $\pi \rightarrow \pi^*$ transition being ruled out). Hypothetically, upon the replacement of the acetate ligand by benzoate, a pure Cu → acetate charge transfer band should noticeably red-shift. Experimentally this is not quite the case. In the solid state, the emission appears at ∼470 nm. The excitation spectrum is centered at ∼355 nm but does not exhibit the vibrational progression observed in Figure 6. In solution, the UV−visible absorption spectrum at room temperature is quasi-identical to that of the acetate analogue, and the emission is centered at ∼455 nm (EtOH, 77 K). This value is red-shifted in comparison to the ∼440 nm value reported for $Cu_2(dppm)_2(O_2CCH_3)^+$ above. The τ_e data are also biexponential (EtOH, 77 K): $I_1 = 80$, $\tau_1 = 67$ μs; $I_2 = 20$, $\tau_2 = 241$ μs. In addition, the TR experiments show the same behavior observed for the acetate complex (Figure 8), except that the λ_{max} of emission is not quite the same (∼530 nm instead of ∼490 nm for the long-wavelength band). There is clear evidence of spectral perturbations arising from the benzoate group, indicating that this group must be involved in the MO's generating the emissive excited states. However the amplitude of these perturbations is not great enough to claim that the Cu → L charge transfer behavior of the excited state is purely located within the CO_2 group. We conclude that the emissive states are mixed Cu → phenylphosphine/acetate charge transfer states.

Acknowledgment. This research was supported by the Natural Sciences and Engineering Research Council of Canada (NSERC) and le Fonds pour la Formation de Chercheurs et l'Aide à la Recherche (FCAR). P.D.H. thanks Professor Mike Baird (Queen's University) for recording the FT-Raman spectrum and Mr. Tom Kwoo (University of Calgary) for fruitful discussions during the DFT calculations.

Supporting Information Available: Listings of crystal data and structure refinement details, all bond lengths and angles, anisotropic displacement parameters, and hydrogen coordinates and isotropic displacement parameters, a figure showing the atomic numbering, listings of EHMO atomic contributions for $Cu_2(PH_3)_4(O_2CH)^+$ and $Cu_2(PH_2(C_6H_5))_4(O_2CCH_3)^+$, MO diagrams for MO's 22−33 for $Cu_2(PH_3)_4(O_2CH)^+$, listings of DFT bond lengths and angles for $Cu_2(H_2PCH_2PH_2)_2(O_2CCH)^+$ and $Cu_2(H_2PCH_2PH_2)_2^{2+}$, a listing of vibrational data for solid $[Cu_2(dppm)_2(O_2CCH_3)]BF_4$, figures showing minimized structures, and excitation and emission spectra of $[Cu_2(dppm)_2(O_2CC_6H_5)]BF_4$ (25 pages). Ordering information is given on any current masthead page.

IC961353V